Research Article

AN ACCURATE AND EFFECTIVE IMPLEMENTATION OF PHYSICAL THEORY OF DIFFRACTION TO THE SHOOTING AND BOUNCING RAY METHOD VIA PREDICS TOOL

Özkan KIRIK*[1], Caner ÖZDEMİR[2]

[1]*Department of Electrical-Electronics Engineering, Mersin University, Ciftlikkoy-MERSIN;*
ORCID: 0000-0002-6996-6239
[2]*Emtech IT Technologies Inc., Mersin Technology Development Zone (Technoscope), Ciftlikkoy, MERSIN;*
ORCID: 0000-0003-2615-4203

ABSTRACT

In this paper, a compact and effective implementation of physical theory of diffraction (PTD) formulation is proposed. The PTD formulation is tailored to recently developed high-frequency radar cross section (RCS) prediction tool; Predics. This PTD implementation is unique such a way that it is specially tailored to shooting and bouncing ray (SBR) technique via ray tracing and field tracing techniques. The detailed derivation of this PTD implementation is formulated and the algorithm steps are given together with its inclusion to Predics. The success and the validity of the proposed PTD implementation to the ray-launching RCS simulator have been tested with several benchmark targets that have either analytical or measured RCS values. Simulated RCS results ensure the accuracy of the proposed diffraction formulation that has been attached to the SBR technique over the test targets given within the paper. To better assess the effect of diffraction phenomenon to the total RCS value, more realistic targets; namely a missile and a helicopter target are analyzed by comparing the RCS results with and without PTD contributions.
Keywords: Radar cross section, computational electromagnetic tools, physical theory of diffraction, shooting and bouncing rays.

1. INTRODUCTION

Calculation of radar cross section (RCS) from electrically large and complex shaped objects has been an attractive problem to electromagnetic (EM) community due to the challenging aspects of the problem [1-5]. The main difficulty comes from the fact that when the size of the target increases in terms of wavelength, the full-method solvers such as method of moments (MoM) [4, 5], integral equation (IE) method [6], finite difference time domain (FDTD) method [7] and finite element method (FEM) require a vast amount of memory and very long computation time that are not practical. To reduce the memory and the computation time necessities, modified versions of full wave methods like multilevel fast multipole algorithm (MLFMA) have also been employed [8, 9]. Although such solvers can improve the performance of the full-wave methods on the order of a couple of times, they are still far beyond to be practical for targets that are in hundreds of

---
* Corresponding Author: e-mail: ozkan@mersin.edu.tr, tel: (324) 361 00 01

wavelengths in three dimensions (3D) to be simulated. To overcome this problem, a clever hybrid approach called Shooting and Bouncing Rays (SBR) has been proposed by Ling et.al. [10] and made it possible to calculate RCS from electrically large and complex shaped objects by enormously reducing both the computation time and the memory metrics. Still, SBR seems to be the only practical technique for calculating the RCS of such bodies that have more than hundreds of wavelengths in one dimension (1D) that results in millions of wavelengths in 3D space. Although several SBR simulation codes have been developed by various researchers [10-12]; recently, a novel, fast SBR-based simulation software called Predics based on an efficient implementation of SBR algorithm by exploiting the parallel computation on multiple central processing units (CPUs) have been developed [13,14].

It is known by the radar community that while SBR is really effective and very successful in estimating surface, single and/or multi-bounce scattering mechanisms, it has a drawback in predicting scattering from structures that have a significant amount of diffracted field energy. Therefore, there is a need for improving the accuracy of SBR tools with the addition of diffracted field calculation from the wedges of the simulated targets. For this purpose; in this work, the accuracy of recently developed RCS prediction code; Predics is being further improved by implementing the physical theory of diffraction (PTD) technique that is added as a new module to Predics.

The organization of the paper is as follows: In the next section, the formulation and the implementation of PTD technique to the SBR technique are presented in detail. In the third section, the validation of the proposed PTD implementation with several benchmark targets is given. In the forthcoming section, RCS results for complex shaped targets such as a navy missile and a helicopter with and without the PTD module are provided to demonstrate the diffraction from the edges to the total RCS. The final section is dedicated to the conclusion of the work and the discussions.

2. FORMULATION AND IMPLEMENTATION OF PTD TECHNIQUE

Since the original Predics code is based on both the physical optics (PO) theory the shooting and bouncing ray (SBR) technique [1,2], implementation of physical theory of diffraction (PTD) solver is required to be in conjunction with the ray tracing and the field theory implementation available within the code. The detailed formulation steps for the implementation of the PTD technique is given below:

i. Prior to PTD implementation, the edges and the wedges of the target's CAD file should be identified. For this work, several tasks as applied in the following order: First, the neighboring triangular patches with at least two common vertices are identified. Then, the outward normal vectors of each neighboring patches are calculated. If these vectors are diverging from each other, this means that the edge is outward directed and should be involved in the PTD calculation. Finally, a maximum edge angle value has to be chosen for edges to be included in PTD calculation. This value is usually selected as 30° in practice in order not to have almost zero PTD contribution energy.

ii. In conjunction with the SBR algorithm, the distance of ray-hit point; d_{hit} to the edge/wedge is calculated by the following formula for any ray included in the ray-tracing module of SBR (see Fig.1);

$$d_{hit} = \frac{|(\vec{P}_0 - \vec{P}_1) \times (\vec{P}_0 - \vec{P}_2)|}{|\vec{P}_2 - \vec{P}_1|} \tag{1}$$

where $\vec{P}_0$ is the vector from the origin to the ray-hit point, $\vec{P}_1$ and $\vec{P}_2$ are the vectors from origin to the start and end points of the edge as demonstrated in Fig.1.
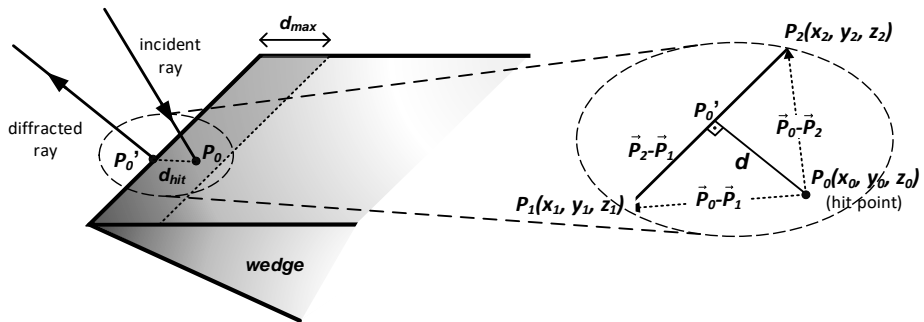
Figure 1. The geometry for PTD implementation

iii. As a general rule of th umb [11], the diffraction contribution of this particular ray is included in PTD result if d_{hit} is less than the maximum permitted distance of $d_{max} = \lambda/10$ where λ is the operational wavelength. In this figure, the point P_0 corresponds to the actual ray hit point near the edge and the point P_0' stands for the approximated ray hit point to be included in the PTD calculation. If $d_{hit} \leq d_{max}$, an equivalent edge-length; d_l is defined [18] with the following equation based on the geometry given in Fig. 1.

$$d_l = \frac{1}{\rho_{rd} \cdot d_{max} \cdot (\cos \theta_{i_1} + \cos \theta_{i_2})} \tag{2}$$

where ρ_{rd} is the ray density of the ray-bunch in SBR implementation that is usually taken as one-tenth of the operational wavelength and θ_{i_1} and θ_{i_2} are the ray incident angles of both wedge surfaces as demonstrated in Fig. 2(a). The edge direction unit vector; $\hat{t}$ is also defined as shown in the same figure. For the PTD calculation, further angles are also defined as illustrated in Fig. 2(b): β_i and β_s are the incident and scattered angles with respect to edge direction unit vector; $\hat{t}$; and $\hat{\imath}$ and $\hat{s}$ are the unit vectors of the incident ray and the scattered ray; respectively.
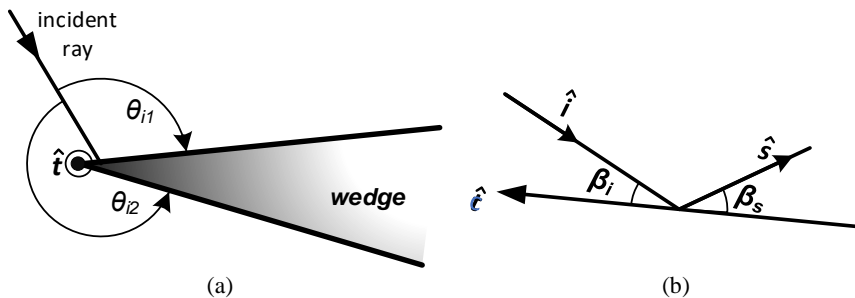

(a) (b)

Figure 2. (a) Incident ray angles with respect to wedge surfaces, (b) Incident and scattered ray angles with respect to the edge direction

For the above set-up, the diffracted electric field; then, can be approximated to the following according to the PTD technique [18]:

iv. For the above set-up, the diffracted electric field; then, can be approximated to the following according to the PTD technique [18]:

$$\vec{E}_d = \frac{e^{-jk|\vec{r}-\vec{r'}|}}{2\pi|\vec{r}-\vec{r'}|} \cdot d_l \cdot \left\{ (D_m - D_\perp')(\vec{E}_i.\hat{a}_{i\parallel}) \cdot \hat{a}_{s\perp} - (D_e - D_\parallel') \cdot \frac{\sin \beta^s}{\sin \beta^i} \cdot (\vec{E}_i.\hat{a}_{i\parallel}) \cdot \hat{a}_{s\parallel} - \right.$$
$$\left. (D_{em}.\sin\beta' - D_x') \cdot \frac{\sin\beta^s}{\sin\beta^i} \cdot (\vec{E}_i.\hat{a}_{i\perp}) \cdot \hat{a}_{s\parallel} \right\} \tag{3}$$

where $\vec{E}_i$ is the incident electric field; $\hat{a}_{i\parallel}$ and $\hat{a}_{i\perp}$ are the unit vectors parallel and normal to the incident ray direction as defined in (4a). In a similar manner, $\hat{a}_{s\parallel}$ and $\hat{a}_{s\perp}$ are defined as the unit vectors parallel and normal to the scattered ray direction as given in (4b).

$$\hat{a}_{i\perp} = \frac{\hat{t} \times \hat{\imath}}{|\hat{t} \times \hat{\imath}|}$$
$$\hat{a}_{i\parallel} = \hat{\imath} \times \hat{a}_{i\perp} \tag{4a}$$

$$\hat{a}_{s\perp} = \frac{\hat{t} \times \hat{s}}{|\hat{t} \times \hat{s}|}$$
$$\hat{a}_{s\parallel} = \hat{s} \times \hat{a}_{s\perp} \tag{4b}$$
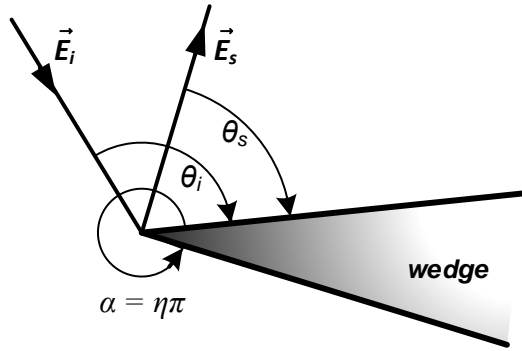

Figure 3. Incident and scattered ray angles with respect to lit-surface of the wedge

v. For the field tracing part of the SBR implementation; incident electric field vector; $\vec{E}_i$ and scattered electric field vector; $\vec{E}_s$ make angles of θ_i and θ_s to the lit facet of the edge as illustrated in Fig.3 where $\alpha = \eta\pi$ is the wedge angle. Diffraction coefficients of D_e, D_m, D_{em} are defined as given in (5a); whereas PO-based coefficients are as in (5b).

$$D_e = \frac{\frac{1}{n}.\sin\frac{\theta^i}{n}}{\cos\frac{(\pi-\alpha_1)}{n} - \cos\frac{\theta^i}{n}} + \frac{\frac{1}{n}.\sin\frac{\theta^i}{n}}{\cos\frac{(\pi-\alpha_2)}{n} + \cos\frac{\theta^i}{n}}$$

$$D_m = \frac{\sin\theta^s}{\sin\theta^i} \cdot \frac{\frac{1}{n}.\sin\frac{(\pi-\alpha_1)}{n}}{\cos\frac{(\pi-\alpha_1)}{n} - \cos\frac{\theta^i}{n}} + \frac{\sin(n\pi-\theta^s)}{\sin\alpha_2} \cdot \frac{\frac{1}{n}.\sin\frac{(\pi-\alpha_2)}{n}}{\cos\frac{(\pi-\alpha_2)}{n} + \cos\frac{\theta^i}{n}} \tag{5a}$$

$$D_{em} = \frac{K}{\sin\beta^i}\left[\frac{\cos\theta^s}{\sin\alpha_1} \cdot \frac{\frac{1}{n}.\sin\frac{(\pi-\alpha_1)}{n}}{\cos\frac{(\pi-\alpha_1)}{n} - \cos\frac{\theta^i}{n}} + \frac{\cos(n\pi-\theta^s)}{\sin\alpha_2} \cdot \frac{\frac{1}{n}.\sin\frac{(\pi-\alpha_2)}{n}}{\cos\frac{(\pi-\alpha_2)}{n} + \cos\frac{\theta^i}{n}}\right]$$

$$D'_\perp = -\frac{\sin\theta^s}{\cos\alpha_1 + \cos\theta^i}$$

$$D'_{//} = -\frac{\sin\theta^i}{\cos\alpha_1 + \cos\theta^i} \qquad (5b)$$

$$D'_x = -\text{K} \cdot \frac{\cos\theta^s}{\cos\alpha_1 + \cos\theta^i}$$

where parameters K, $\sin\alpha_1$ and $\sin\alpha_2$ are below in (5).

$$\text{K} = \sin\beta^s \cdot \cot\beta^i - \sin\beta^i \cdot \cot\beta^s$$

$$\sin\alpha_1 = \frac{\sqrt{\sin^2\beta^i - \sin^2\beta^i \cdot \cos^2\theta^s}}{\sin\beta^i} \qquad (6)$$

$$\sin\alpha_2 = \frac{\sqrt{\sin^2\beta^i - \sin^2\beta^s \cdot \cos^2(n\pi - \theta^s)}}{\sin\beta^i}$$
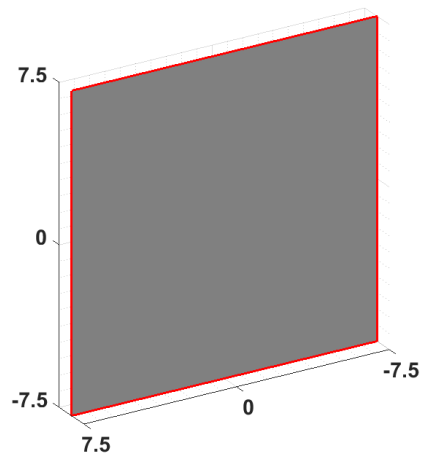
3. SIMULATION RESULTS

The above formulation of the PTD technique has been coded in Microsoft .NET framework with C# development environment and implemented to Predics. Afterwards, various benchmark targets have been tested to be able to assess and evaluate the performance of Predics code with the improved formulation of the PTD technique. Namely; rectangular plate, rectangular dihedral corner reflector, rectangular trihedral reflector and cone-sphere targets have been tested in order.
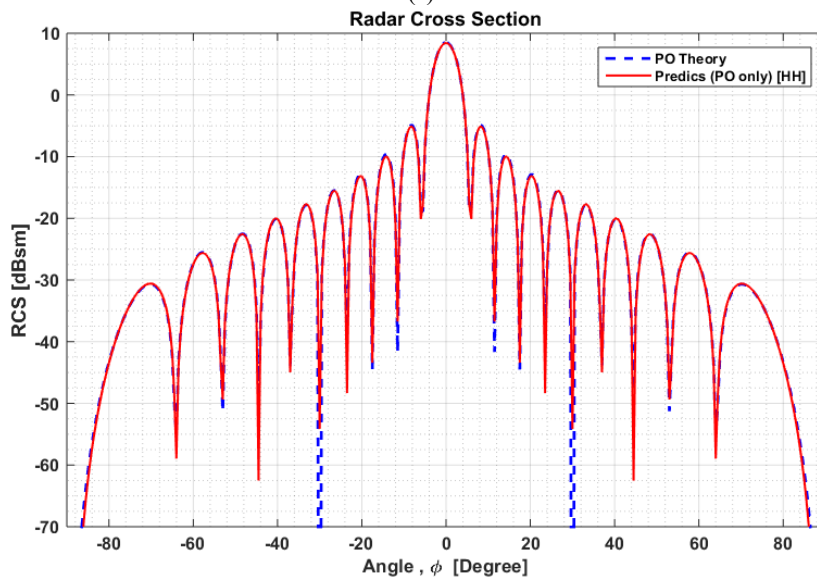
3.1. Rectangular plate

The most common target, often used in benchmarking tests, is the perfectly conducting rectangular plate whose geometry is shown in Fig. 4(a). The analytical solution of this geometry for PO theory is known for years and can easily be reached in [15]. First, the PO simulation of the target by using Predics was performed to validate the PO calculation of Predics. For this purpose, a PEC plate of 15 cm x 15 cm is considered and the monostatic RCS simulation of horizontal polarization at 6 GHz was carried out at for the azimuth angles from -90° to 90° for a total of 361 discrete angle points. The ray density for the ray-launching process is chosen to be 10 rays/wavelength. The results are shown in Fig. 4(b) where theoretical RCS is drawn in blue dashed line and the simulation result is given in solid red line. Almost perfect agreement between the PO theory and the PO solver simulation of Predics can be easily deduced from the figure. Having the PO solver exactness of Predics in hand, the performance after the PTD implementation is tested with real RCS measurement versus full PO+PTD solver of Predics. The measured data is gathered from [18] for the target shown in Fig 4(a). The measured monostatic RCS of the rectangular plate was measured in HH polarization for the same frequency of 6 GHz and the same azimuth look angles between -90° and 90°. Predics's PO+PTD simulation of the geometry for the same frequency and angles set-up have been performed. The edges of the geometry, detected by Predics, was automatically drawn as red solid lines on the CAD file as it can be viewed in Fig. 4(a).

The measured result is plotted in Fig. 4(c) as blue dashed line whereas the simulation result Predics is drawn as red solid line in the same figure. Almost perfect match between the measured RCS and the simulated RCS with PO+PTD solver can be easily observed from the figure that demonstrates the exactness of Predics's electromagnetic calculation ability for both scattered and diffracted electric fields.
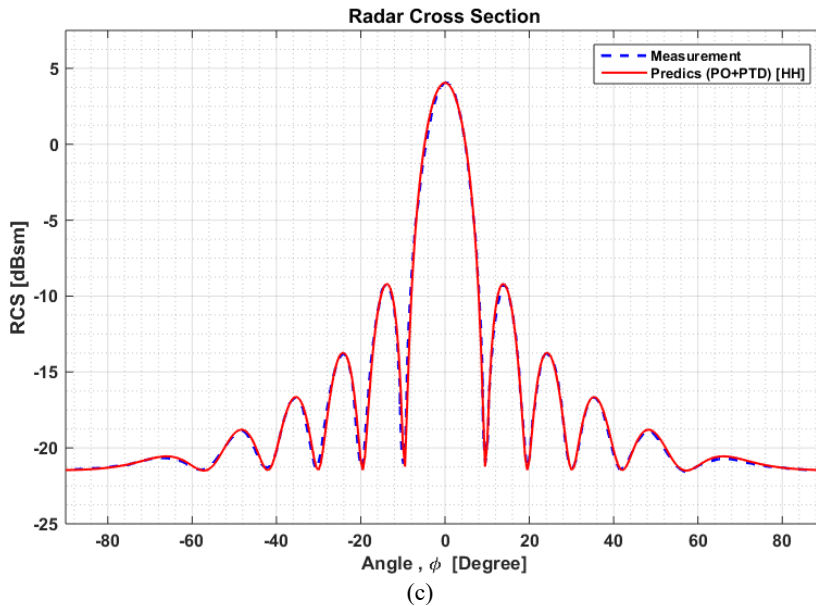
(a)

(b)

(c)

Figure 4. (a) Rectangular plate geometry, (b) RCS results by PO theory and Predics simulation (PO) of plate target, (c) RCS results for the measured and Predics simulation (PO+PTD) of plate

3.2. Rectangular dihedral corner reflector:

As the second benchmark target, a perfectly conducting rectangular dihedral corner reflector (DCR) with square plates of lengths $a = b = 5.6088\lambda$ is taken into consideration as its CAD file can be viewed in Fig. 5(a). For this particular object, a measured monostatic RCS data is available for the whole azimuth angles ($\theta = 90°$) at 9.4 GHz in [18]. Unlike previous benchmark object, DCR has the feature of supporting multi-bounce mechanisms due to its natural geometrical orientation. In the Predics simulation; therefore, all PO, SBR and PTD solvers have been used to calculate the backscattered RCS value. Both the measurement and simulation results are presented in Fig.5(b): While Griesser's measurement for the VV polarization is plotted as blue dotted line, Predics's PO+SBR+PTD simulation result is given as red solid line. Very good agreement between the measured RCS results by [18] and the calculated RCS results is obvious from the figure which in turn demonstrates the correctness of the proposed PTD implementation for the calculation of electromagnetic scattering/diffraction from the single and double bounce electromagnetic mechanisms.
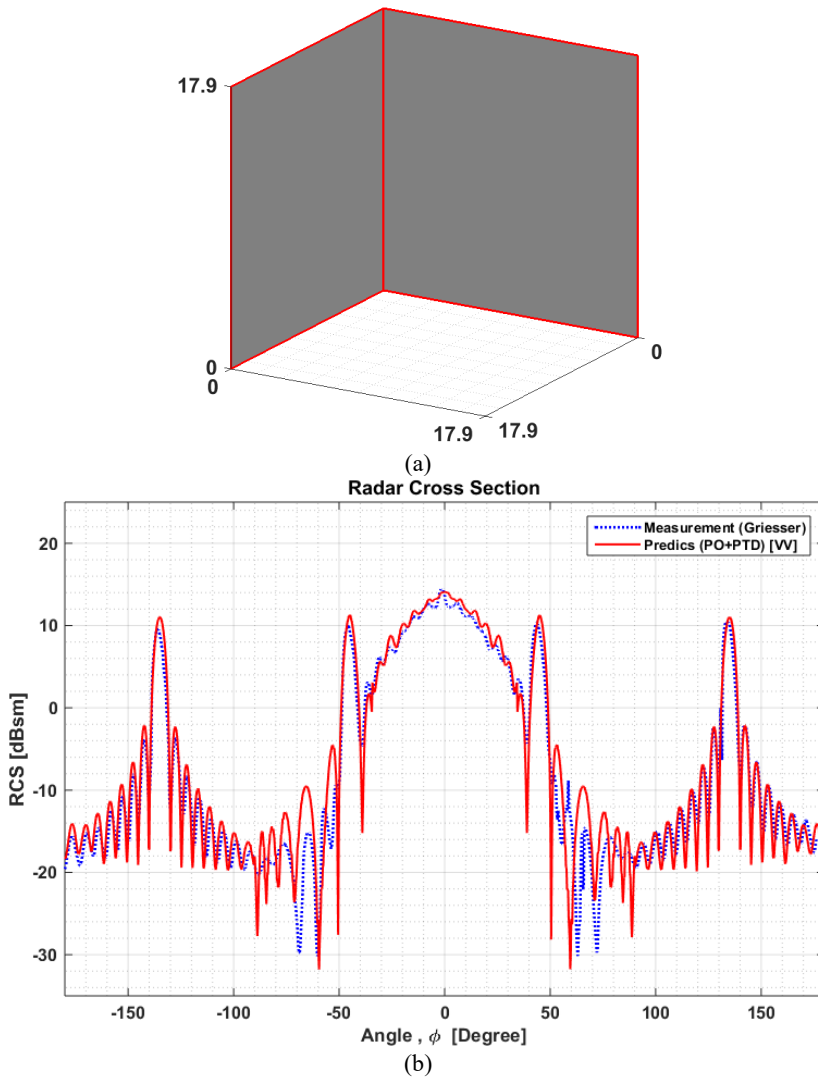
(a)

(b)

Figure 5. (a) Rectangular dihedral corner reflector geometry, (b) Angular RCS results comparison with respect to the measurement of [18], Predics simulation (PO+SBR+PTD)

3.3. Rectangular trihedral corner reflector:

Another benchmark object that is widely used is electromagnetic problems is the trihedral corner reflector (TCR). For the test-object, a TCR with equal corner lengths of 40 cm is used as illustrated in Fig. 6(a) and the Predics's RCS prediction accuracy has been tested over frequencies in this numerical experiment. Again, the detected edges are automatically drawn as red lines on the CAD view of the object as seen from the figure. Since there is no measured RCS result available in the literature for any TCR object, Predics's results have been compared with simulated results of the well-known commercial EM simulators; namely Altair FEKO [19] and

CST Microwave Studio [12]. For this experiment, the backscattered RCS simulations at VV polarization have been carried out by using FEKO (UTD solver), CST (Asymptotic solver) and Predics (PO+SBR+PTD solver) for the frequencies between 1 GHz and 9 GHz. The RCS results of these three simulators are plotted in Fig. 6(b) where very good agreement between the three results can be easily noticed.
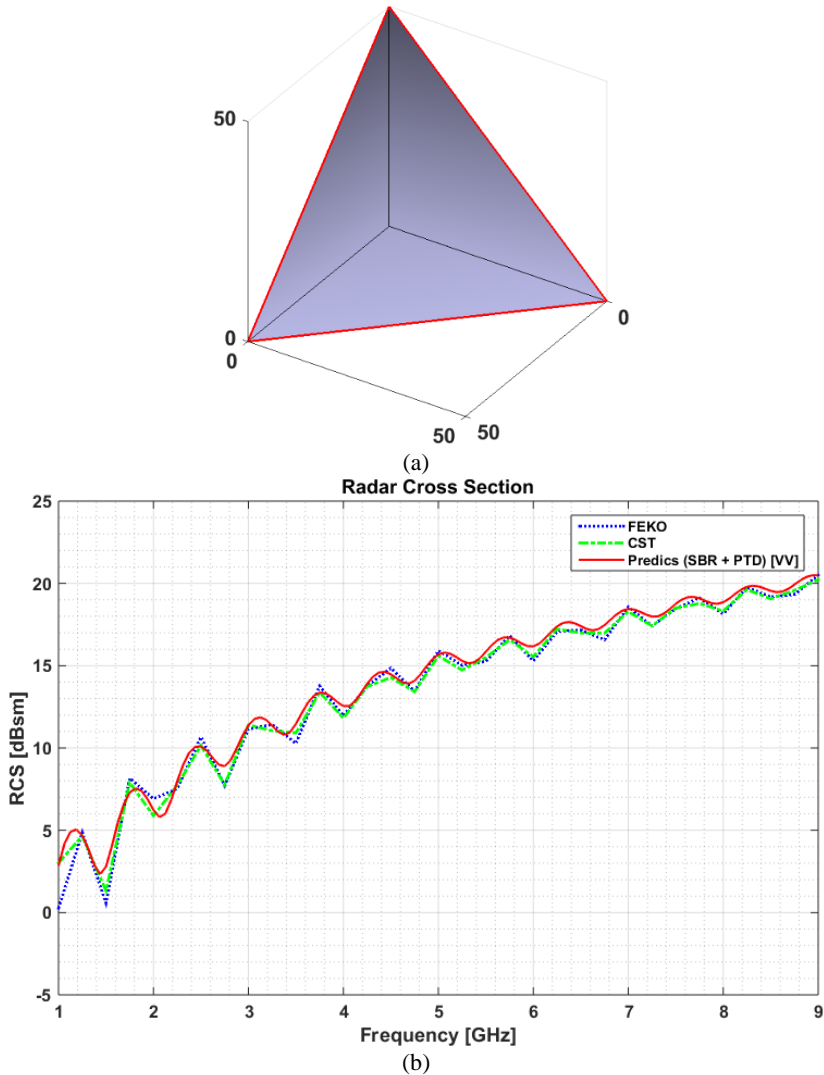

(a)

(b)

Figure 6. (a) Rectangular trihedral corner reflector geometry, (b) Spectral RCS results for FEKO (PO+PTD), CST (Asympotic) and Predics (PO+SBR+PTD) simulations

3.4. Cone-sphere:

The last test target that is widely used as a benchmark target is RCS validation is the "cone-sphere" with the sphere radius of 74 mm and the cone height of 605 mm [16]. The geometry of the target can be seen in Fig. 7(a). A monostatic RCS measurement of "cone-sphere" geometry at 9 GHz for the whole azimuth angles is available in [16] and plotted in Fig. 7(b) as blue dotted line. Predics's simulation result for the simulation conditions with the PO+PTD solver is given in the same figure as red solid line. A fair comparison between the measured result and the Predics's simulation result is obvious in the figure. To compare the Predics's results with known reliable simulators, Altair FEKO and CST Microwave Studio have also been utilized and the corresponding RCS results are given as green dashed line, black dashed line, respectively. Comparing all these four curves, the following observations are made in order. (i) For the region between 0° and -90° where the incident wave can only see a circular region, all three curves experience a flat RCS behavior around -16 dBsm as expected. (ii) For azimuth look angles between -90° and -180°, the conical part of the geometry interferes with the incoming wave. At a particular angle of -97°, incident electric field experiences specular reflection from the side surface of the cone which shows up as a peak at the RCS curve. Similar to FEKO result, Predics result successfully estimates this peak in accordance with the measurement result of Griesser. (iii) For angles from -100° to -180°, the sphere part of the geometry is not illuminated by the EM wave and the illuminated part (i.e., the cone) do not support the strong scattering mechanisms; rather, only the diffraction fields are generated that have significantly lower energy than the scattered fields. Therefore, RCS levels that are almost 45 dB less than the peak RCS value for this region of look-angle are observed. Similar to Altair FEKO, Predics's RCS simulation produces RCS values that fluctuate between -35 dBsm and -45dBsm. Similar behavior can also be deducted from the measurement result in Fig. 7(b). CST seems to estimate RCS values somewhat lower when compared to FEKO and Predics for this region.
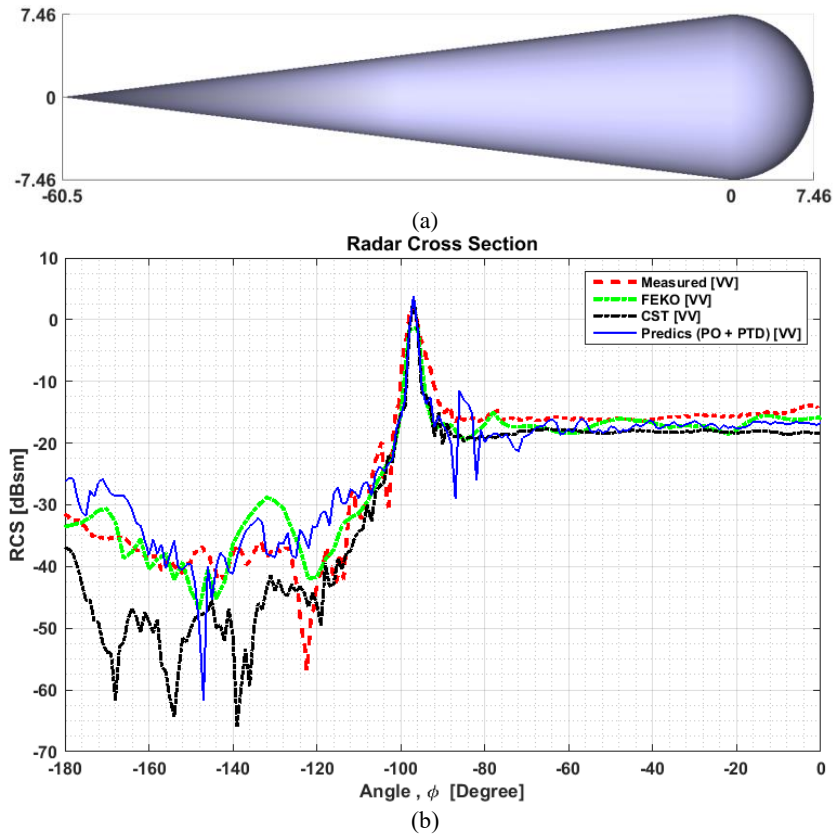
Figure 7. (a) Cone-sphere geometry, (b) Angular RCS results comparison with respect to FEKO simulation (PO+PTD), CST simulation (PO+PTD) and Predics simulation (PO+PTD)

4. EFFECT OF PTD SOLVER

The effect of PTD solver has been demonstrated over a more complex target which is the generic missile whose CAD model is given in Fig. 8(a). The missile has a length of 2168 mm and tails with aperture widths of 48 mm. The edges of the target have been automatically identified by Predics code was drawn as red lines in the GUI screen of Predics as can be viewed from the figure. Firstly, monostatic RCS simulation of the missile target has been performed from the nose-on case; i.e. look-angle of radar towards to the front of the missile, and the frequency is varied from 7.5 GHz to 12.5 GHz for a total of distinct 100 frequency points. In Fig. 8(b), RCS variation versus frequency is plotted both for (PO+SBR) solver and (PO+SBR+PTD solver) that are plotted in blue dashed line and red solid line, respectively. The amount of increase in the total RCS value of the target can be easily seen for the whole frequency band after adding the diffraction components thanks to the PTD solver. It is obvious; therefore, to point out that PTD solver has to be used for structures that have certain amount of edges. Likewise, the missile target geometry in Fig. 8(a) has long distinct edges almost ranging from its nose to tail which in turn boost up the RCS value. To better pinpoint and interpret the locations of diffraction energies, the range profile of the missile target is formed by taking the one-dimensional Fourier transform of the back-scattered electric field of the above-mentioned simulation as [20]

$$E_s(r) = IFT\{E_s(f)\} \tag{7}$$

The resultant range profile of the target is plotted in Fig. 8(c) where the range profile for (PO+SBR) solver is plotted as the blue dashed line and the range profile for (PO+SBR+PTD) solver is plotted red solid line. This figure exactly shows off the regions where on the target are responsible for the diffracted energies that influenced the total RCS value. One can easily notice from Fig. 8(c) that the PTD solver only increased the total range profile value only for the regions where there are edges as expected. This region spreads from 50 cm to -108 along the range axis. Sharp peaks are also observed for the points of kinky changes along the edges. These points are drawn to be matched for the sudden peaks in the range profile plot in the figure. The exact match between the locations of edge corners and the locations of RCS peaks demonstrates that the diffracted field phase calculation is perfectly successful.
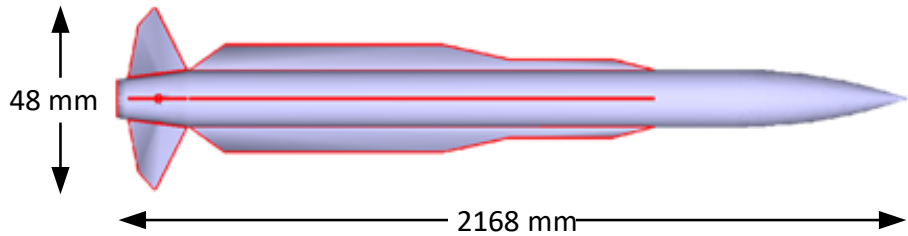
(a)
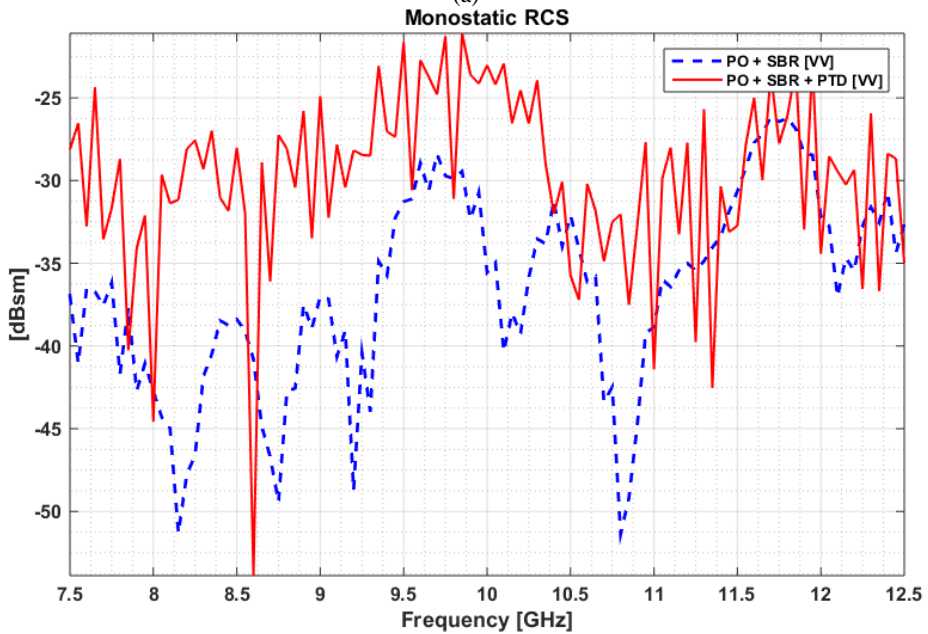
(b)
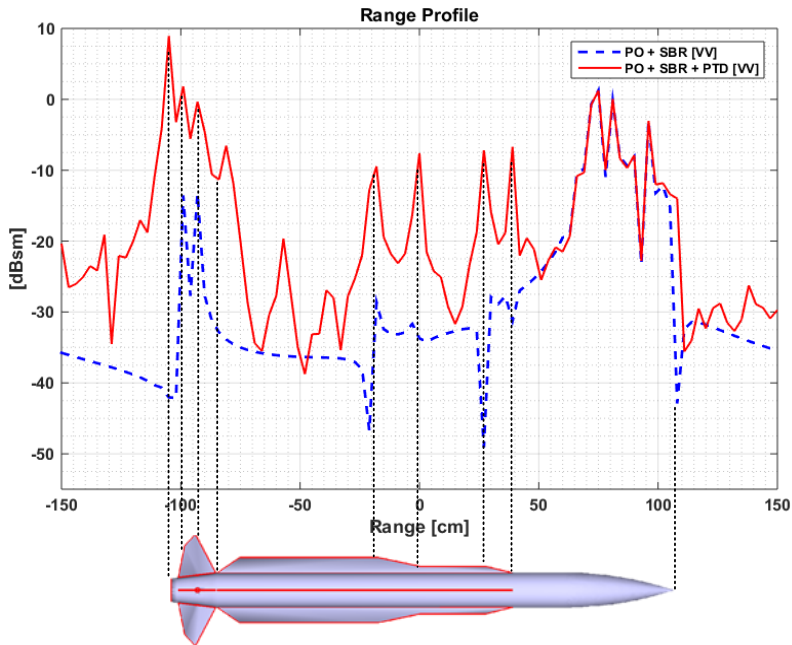
(c)

Figure 8. (a) CAD file view of generic navy-missile target and (b) monostatic RCS results for (PO+SBR) and (PO+SBR+PTD) solvers (c) range profiles for (PO+SBR) and (PO+SBR+PTD) solvers

5. CONCLUSIONS AND DISCUSSIONS

In this work, a novel PTD methodology has been developed and implemented for the recently developed high frequency computational electromagnetic simulator of Predics that can accurately calculate the electromagnetic scattering and RCS from electrically large and complex targets at microwave frequency bands. The fundamental formulation of the PTD and the steps of the implementation procedures have been shared. The PTD implementation has been assessed by the help of various benchmark objects. The RCS outcome of Predics with (PO+SBR+PTD) solver have demonstrated almost a perfect performance in all of these benchmark targets. With the addition of PTD solver, Predics has gained the ability to calculate the diffracted fields together with scattered fields from any target with good fidelity. This has been demonstrated within the paper by comparing the RCS results of Predics that were compared to other strong commercially available CEM tools of CST Microwave Studio and Altair FEKO.

The effect of diffracted fields has been demonstrated with the missile target given in the fourth section. This example surely shows how the diffraction energies can contribute to the total scattered electric field value. Although the scattered fields seem to be significantly responsible for the total backscattered energy for practical targets of arbitrary shape, diffracted fields can contribute more than scattered fields when sharp edges/wedges are present within the geometry as demonstrated in missile example. Therefore, the availability of PTD solver is very crucial and important for the accurate calculation of RCS values from targets of any shape.

Acknowledgments

REFERENCES

[1]   Ling H, Chou RC, Lee SW. Shooting and bouncing rays: calculating the RCS of an arbitrarily shaped cavity, IEEE T Antenn Propag 1989; 37: 194–205.

[2]   Ling H, Lee SW, Chou RC. High frequency RCS of open cavities with rectangular and circular cross-sections. IEEE T Antenn Propag 1989; 37: 648–654.

[3]   Youssef NN. Radar cross section of complex targets. Proc IEEE 1989; 77: 722–734.

[4]   Weinmann F, Nitschkowski J. A SBR simulator with GO-PO for calculating scattered fields from coated surfaces. In: Proceedings of the 4th European Conference on Antennas and Propagation; 12–16 April 2010, Barcelona, Spain. pp. 1–4.

[5]   Jin JM, Ling F, Carolan ST, Song JM, Gibson WC, Chew WC, Lu CC, Kipp R. A hybrid SBR/MoM technique for analysis of scattering from small protrusions on a large conducting body. IEEE T Antenn Propag 1998; 49: 1349–1357.

[6]   Liu K., Balanis C.A., Griesser T. An integral equation solution for the RCS of large dihedral corner reflectors. Digest on Antennas and Propagation Society International Symposium 1989, San Jose, CA, USA, USA

[7]   Luebbers R, Steich D, Kunz K. FDTD calculation of scattering from frequency-dependent materials. IEEE T Antenn Propag 1993; 41: 1249–1257.

[8]   Manyas A, Gürel L. Memory-efficient multilevel physical optics algorithm for fast computation of scattering from three-dimensional complex targets. In: Computational Electromagnetics Workshop; 30–31 August 2007; İzmir, Turkey. pp. 26–30.

[9]   Pan XM, Pi WC, Yang ML, Peng Z, Sheng XQ. Solving problems with over one billion unknowns by the MLFMA. IEEE T Antenn Propag 2012; 60: 2571–2574

[10]   Ling, H., Chou, R.C., and Lee, S.W., Shooting and bouncing rays: Calculating the RCS of an   arbitrarily shaped cavity, IEEE Trans Anten Propag 1989, 37:194-205.

[11]   Weinmann F. Ray tracing with PO/PTD for RCS modeling of large complex objects. IEEE T Antenn Propag 2006; 54: 1797–1806.

[12]   CST – Electromagnetic Simulation Software Available at https://www.cst.com/

[13]   Özdemir, C., Yılmaz, B., and Kırık, Ö., "pRediCS: A new GO-PO based ray launching simulator for the calculation of electromagnetic scattering and RCS from electrically large and complex structures" Turkish Journal of Electrical Engineering & Computer Sciences, Vol. 22, 1255 – 1269 (2014).

[14]   Özdemir, C., Yılmaz, B., Kırık, Ö., Sütcüoğlu, Ö., "A Fast and Efficient RCS Calculation and ISAR Image Formation Tool: pRediCS", 10th European Conference on Synthetic Aperture Radar (EUSAR 2014), Berlin, 2014. (poster)

[15]   Balanis CA. Advanced Engineering Electromagnetics. 2nd ed. New York, NY, USA: Wiley, 2012.

[16]   Griesser T, Balanis CA, Liu K. RCS analysis and reduction for lossy dihedral corner reflectors. P IEEE 1989; 77: 806–814.

[17]   O'Donnell R. M., Radar Systems Engineering, IEEE New Hampshire Section, 2010.

[18]   Griesser T, Balanis C. Backscatter analysis of dihedral corner reflectors using physical optics and the physical theory of diffraction. IEEE T Antenn Propag 1987; 35: 1137–1147.

[19]   FEKO   Suite   6.0.   EM   Software   and   Systems.   Available   at https://altairhyperworks.com/product/FEKO

[20]   Ozdemir C. Inverse Synthetic Aperture Radar Imaging with MATLAB Algorithms. New Jersey, USA: John Wiley & Sons, 2012.

Chemistry &Chemical Engineering Articles